Iranian Journal of Chemistry and Chemical Engineering (IJCCE)

Dissolution Kinetics for Colemanite Ore in Propionic Acid Solutions Saturated with Pyrite Roasting Gas

Mücahit Uğur[1]

Department of Chemical Engineering, Faculty of Engineering, Çankırı Karatekin University, Çankırı, TURKEY

ABSTRACT: *In this study, the dissolution kinetics for colemanite in propionic acid solutions saturated with pyrite roasting gas were investigated in a mechanically mixed system. The parameters were determined as temperature, particle size, solid/liquid ratio, acid concentration, gas flow rate, and* stirring *speed. The dissolution rate increased with increasing temperature, acid concentration, and pyrite roasting gas flow rate, while it reduced with increases in particle size and solid/liquid ratio. Compared to other parameters, stirring speed was found to have no significant effect on dissolution rate. The experimental data obtained were applied to homogeneous and heterogeneous reaction models by linear regression using the Statistica 10 Package Program to derive the appropriate model for the dissolution kinetics of colemanite. As a result, the dissolution rate was found to be controlled by a modified Avrami model. The activation energy for the process (E) was 38.66 kJ/mol and the Arrhenius constant was calculated as* $9.6*10^4$.

KEYWORDS: *Colemanite, Pyrite Roasting Gas, Dissolution Kinetics, Propionic Acid*

[1]*Corresponding author. E-mail address: m.ugur@karatekin.edu.tr, Tel: +90-376-2189500/7909.*

INTRODUCTION

Boron minerals are found as natural compounds containing different proportions of boron oxide (B_2O_3) in their structure. Though more than 230 boron minerals are found freely in nature, only a few are important in commercial and industrial terms [1]. These are colemanite ($Ca_2B_6O_{11}.5H_2O$), kernite ($Na_2B_4O_7.4H_2O$), tincal ($Na_2B_4O_7.10H_2O$), and ulexite ($NaCaB_5O_9.8H_2O$) [2, 3]. Turkey is in first place holding 72.2% of the world's boron reserves [4]. Colemanite deposits are located in Emet-Kütahya, Bigadiç-Balıkesir, and Kestelekte-Bursa in Turkey [5]. Apart from Turkey, the USA and China, followed by Russia, Peru, Bolivia, Chile, and Argentina, are countries with boron reserves [6].

Boron is used in many areas such as for the preparation of chemicals, disinfectants and medications in medicine and pharmaceutical industry [7, 8], composite material and glass [9], fiberglass [10], agriculture and fire retardants [11], high-quality steel, heat resistant polymers [12], cleaning and whitening [13], in cosmetic production, leather and dye processing [14], nuclear engineering [15], in fuel for rocket engines, and hard and refractory alloys [16].

Boric acid, the most principal boron compound is produced by the reaction of colemanite ore with sulfuric acid in the temperature range of 88-92^oC, under atmospheric pressure in the industry as shown by reaction 1[17].

$$Ca_2B_6O_{11}.5H_2O_{(s)} + 2H_2SO_{4(aq)} + 6H_2O \rightarrow 6H_3BO_{3(aq,s)} + 2CaSO_4.2H_2O_{(s)} \quad (1)$$

As sulfuric acid is a powerful acid, it reacts with clay and other minerals within the ore, not just with colemanite ore. Thus, increasing impurities like Ca^{+2} and Mg^{+2} in the solution, especially, cause a reduction in boric acid quality in boric acid production [14, 18]. In addition, there is a loss of boron, which contains approximately 3-6% B_2O_3 mixed with the by-product gypsum (borogypsum) clay [13]. In Turkey, while producing $3.3*10^5$ tons of boric acid in this method, $6.5*10^5$ tons of borogypsum are generated annually [14]. This borogypsum is stored in open artificial ponds however, it causes pollution of soil, water, and the environment through dissolution by rainwater [1, 18]. Additionally, for completion of the reaction between colemanite and H_2SO_4, a little excess acid is added. Due to this excess acid and the solubility of the borogypsum formed, excess sulfate ions are observed in the main solution. This situation causes sulfate impurities in crystallized boric acid, an impurity unwanted in many industries that boric acid. For this reason, there is a need to research new methods to reduce this impurity.

Information related to the activation energies and rate control models for these dissolution processes is summarized in Table 1.

Table 1: Summary of dissolution kinetics for colemanite using different leach solutions

Leach Solution	Activation energy kJ/mol	Rate control model	Reference
Di ammonium hydrogen phosphate	42.10	First-order pseudo homogenous	[1]
Potassium dihydrogen phosphate	41.88	Chemical reaction controlled	[18]
Methanol	51.4	Second-order pseudo homogenous	[12]
Oxalic acid	27.88	First- order pseudo homogenous	[19]
Ammonium carbonate	59.03	First-order pseudo homogenous	[20]
Ammonium hydrogen sulfate	32.66	Product film diffusion controlled	[14]
Ammonium sulfate	59.03	First-order pseudo homogenous	[20]
Perchloric acid	46.76	Chemical reaction controlled	[21]
Ammonium sulfate	40.46	Chemical reaction controlled	[11]
Sulfuric acid	41.40	Product film diffusion controlled	[22]
Sulfur dioxide gas	50.14	Avrami model	[23]
Citric acid	28.65	Product film diffusion controlled	[24]
Oxalic acid	39.71	Product film diffusion controlled	[25]
Sulfur dioxide gas	39.53	Chemical reaction controlled	[26]
Sulfuric acid	28.96	Surface chemical reaction	[27]
Phosphoric acid	53.9	Surface chemical reaction	[27]
Chlorine	35.56	Chemical reaction controlled	[28]
Acetic acid	51.49	First-order pseudo homogenous	[29]
Ammonium chloride	89	Second-order pseudo homogenous	[30]

The main problem in the production of boric acid from colemanite ore with sulfuric acid is that due to its strong acidity, it easily dissolves impurities such as Ca^{2+} and Mg^{2+} in the colemanite ore and causes impurities in the product together with SO_4^{2-} resulting from its structure [11, 12]. The dissolution of dolomite ($CaCO_3$. $MgCO_3$) containing Ca^{2+} and Mg^{2+}, limestone ($CaCO_3$) containing Ca^{2+} and clayey structures containing Mg^{2+} causes impurities in boric acid and reduces product quality. In addition, a significant amount of borogypsum (gypsum) formed as a by-product is stored in artificial lakes and this causes environmental pollution [12]. To minimize these effects, the colemanite ore must be treated with an acid that does not or slightly reacts with minerals other than

colemanite, and this acid must be stronger than boric acid [11]. For this purpose, acetic acid, propionic acid, and similar acids with longer carbon chains can be used [31]. In this study, PRG-saturated aqueous solutions of propionic acid are used to dissolve colemanite. Since propionic acid is not as strong as sulfuric acid, it cannot dissolve the main sources of impurities in colemanite. This creates a significant advantage for the production of higher-purity boric acid. Thus, it is predicted that this acid is feasible because it does not impose an extra economic burden on removing impurities in the product. The dissolution temperature of colemanite is between 88-92°C and the vapor pressure of propionic acid is lower than other acids during the reaction, which provides an advantage in terms of acid loss and odor problems. In addition, while boric acid is produced from sulfuric acid, borogypsum, which causes environmental pollution, is prevented from polluting nature. On the contrary, calcium sulfite ($CaSO_3.{}^1/_2H_2O$) which will be obtained instead of borogypsum, is a substance that can be evaluated in the industry [23, 26]. In addition, there is no loss of propionic acid in the production of boric acid from colemanite with propionic acid.

This study investigates the dissolution kinetics of colemanite in propionic acid (PA) solutions saturated with SO_2 in pyrite roasting gas (PRG), and a mathematical expression representing the dissolution process is derived.

EXPERIMENTAL SECTION

Materials

Colemanite ore used in the research was obtained from boron deposits in the Emet-Kütahya region of Turkey. The chemical analysis results determined with spectrophotometric and gravimetric methods for this ore found it contained 34.21% B_2O_3, 19.24% CaO, 14.66% H_2O (water in the crystal structure of colemanite), 1.72% MgO and 0.71% humidity. The remaining proportions comprise clay minerals, CO_2, and SiO_2.

After breaking and grinding with the aid of an ore crusher, fractions were separated to 100-150 µm, 150-250 µm, 250-400 µm, and 400-600 µm using ASTM E11 standard sieves, and these fractions were used in experiments. In the kinetic calculations, the arithmetic average of these particle sizes was used.

To determine the phase composition of colemanite ore, X-Ray diffraction (XRD) was used, while the basic composition of colemanite was determined with a scanning electron microscope (SEM). XRD analysis was given in Figure 1, with SEM images given in Figure 2.

X-Ray diffractogram of colemanite ore and solid product formed during the reaction was analyzed with Rigaku MiniFlex brand X-Ray diffraction device, SEM image was analyzed with LEO 1430 VP model SEM device.

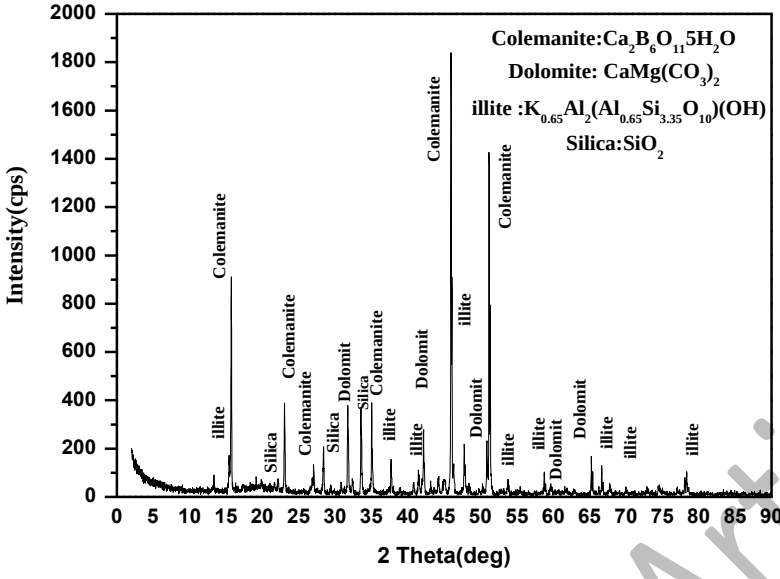

Fig. 1: XRD analysis of colemanite ore

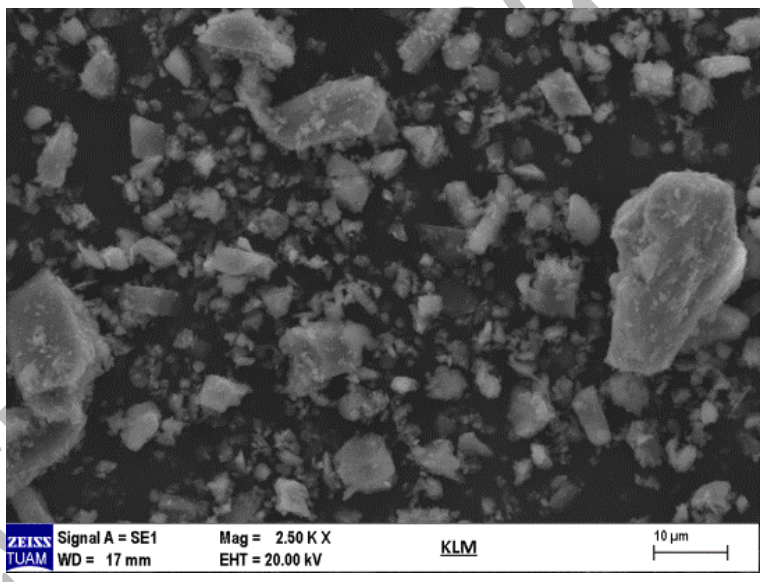

Fig. 2: SEM image of colemanite ore

PA used in this study had 99% purity and was purchased from Merck. PA is a weak acid with an acid constant of $1.34x10^{-5}$. The fact that the boiling point of this acid was high compared to other similar acids and that it allows it to work at high temperatures makes it an alternative in the production of boric acid. There were clayey structures, dolomite ($CaCO_3$, $MgCO_3$), and limestone ($CaCO_3$), which are sources of Ca^{+2} and Mg^{+2} in ore in addition to the Ca content of colemanite. Since PA is not a strong acid like H_2SO_4, it cannot completely dissolve these structures, which are the source of impurities in colemanite, and provides a significant advantage for producting higher-purity boric acid. Thus, it can be said that this acid is more feasible as it does not bring an extra economic burden to remove the impurity in the product. Moreover, the propionic acid used in this study was not

consumed and was recycled at the end of the process. In this regard, it may be necessary to compare the cost of PRG, not sulfuric acid and propionic acid.

PRG is obtained by roasting pyrite. It is cleaned from dust and elements that may negatively affect the sulfuric acid process, such as Hg, As, Cu, and Fe. It is then used in the production of sulfuric acid. In this study, after PRG is cleaned, other stages of sulfuric acid production are skipped and aqueous solutions of propionic acid are used to obtain boric acid from colemanite. Therefore, the cost per ton is significantly lower than producing boric acid with conventional sulfuric acid.

PRG is formed during the roasting of pyrite (FeS_2), an iron ore, in the industry, as shown in Equation 2,

$$2FeS_{2(s)} + {}^{11}/_{2}\, O_{2(g)} + 22N_{2(g)} \rightarrow Fe_2O_{3(k)} + 4SO_{2(g)} + 22N_{2(g)} \quad (2)$$

PRG, which partially contains O_2, is used in the production of sulfuric acid after it is purified from dust [32].

PRG with a composition of 13%SO_2, 7%O_2, and 80% N_2 used in this study is supplied from Linde company and was prepared synthetically.

When SO_2 is used instead of sulfuric acid, it creates environment-friendly $CaSO_3$, which has many uses in the industry and has high added value, instead of borogypsum, which causes environmental problems as a by-product [23, 26], and also ensures that the amount of sulfate in boric acid is at a minimum level.

Method

During experiments, reaction temperature(T), solid/liquid ratio(S/L), particle size(D), PA concentration(C), PRG flow rate(GD), and stirring speed(MR) were determined as parameters. The parameters and their levels are given in Table 2. Experimental parameters and levels were determined by considering the literature and preliminary test results.

Table 2: Parameters used in experiments and their levels

	Parameters	Levels
A	Reaction temperature (K)	283, 293, 303*, 313, 323
B	Particle size (µm)	100-150, 150-250, 250-400*, 400-600
C	Solid/fluid ratio (g/L)	20, 40*, 60, 80
D	PA concentration (%)	0%, 2.5%, 5%*, 10%
E	PRG flow (mL/min)	50, 100*, 150
F	Stirring speed (rpm)	300, 400*, 500

* While the effect of one parameter was investigated, the levels of the other parameters were kept constant.

To more clearly see the effect of a particular parameter on the dissolution of colemanite, the levels of other parameters marked with an asterisk were kept constant. These fixed levels were chosen except for the maximum and minimum values. The experimental design table prepared accordingly is given in the Appendix.

Experimental procedure

Experiments were performed in a 500 ml double-walled batch glass reactor at atmospheric pressure. The solution temperature in the reactor was set on a fixed temperature circulator (Polyscience brand SD20R-30-A12E model) and the reactor contents were mixed with a mechanical stirrer (SCILOGEX brand OS20-Pro model). The desired concentrations of PA in water were placed in the reactor and the reactor content was heated to the desired temperature, then, after the PRG was passed through a coke tower for drying, it was transferred to a digital flowmeter (Aalborg brand GFC17 model), and from there it was sent to the reactor stirred at a certain speed. After the solution was saturated with SO_2, a certain amount of colemanite ore was added and the reaction began. During the reaction, PRG flow was continued. The setup used for the experiments is given in Figure 3.

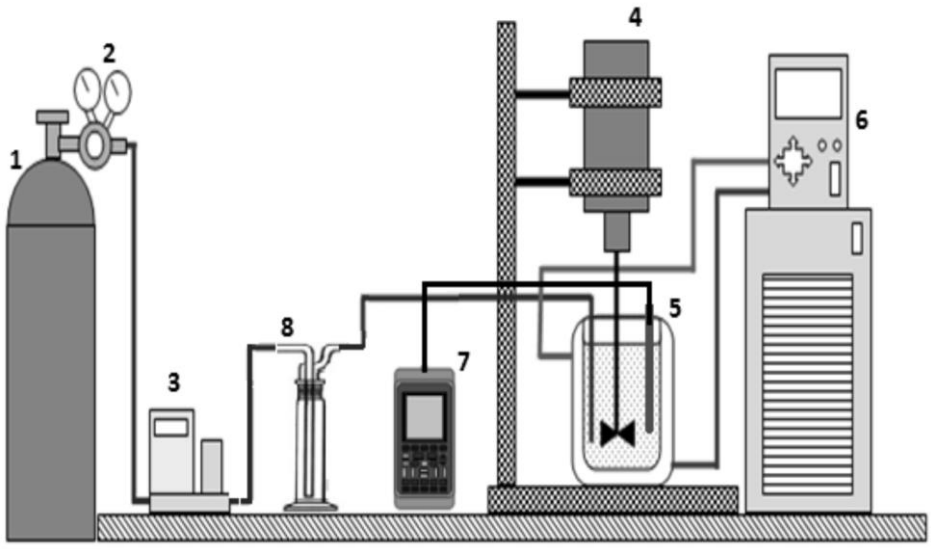

Fig. 3: Set up used in experiments

1- PRG cylinder 2- Pressure-reducing regulator 3- Digital flowmeter 4- Mechanical stirrer with tachometer 5- Jacketed glass reactor 6- Fixed temperature circulator 7- pH meter 8- Humidifying column

Analysis, calculations, and modeling

During the experiment, 11 test samples were taken at different times within 60 minutes. A certain amount of suspension solution was quickly filtered with quantitative filter paper with a pore diameter of 2.5 µm. 2 mL of the filtered solution was taken and the volume was completed to 100 mL. B_2O_3 analyses were performed on samples prepared by filtering from the reactor at certain time intervals. For B_2O_3 or boric acid detection, after neutralizing reactant acids (H_2SO_3 and propionic acid) contained in the solution with a NaOH solution, boric acid within the analysis sample, which is a weak acid and cannot be accurately titrated with bases, was transformed to a moderate acid ($Ka \approx 10^{-5}$) with $HOB[CH_2OH(CHOH)_4CH_2O]_2$ chemical formula by the addition of mannitol

[$CH_2OH(CHOH)_4CH_2OH$)] and it was titrated with 0.05M NaOH solution [7]. The amount of B_2O_3 passing into the solution;

$$B_2O_3\ amount(g) = \frac{VxMx35}{1000}$$

(3)

by equation 2, the dissolution fraction of colemanite is;

$$X_{B_2O_3} = \frac{Amount\ of\ B_2\ O_3\ passing\ into\ solution\ \ from\ colemanite\ (g)}{Amount\ of\ B_2\ O_3\ in\ colemanite\ (g)}$$

(4)

calculated with the equation 4. Here, V is the volume (mL) of the NaOH solution consumed in the titration, M is the molarity of the NaOH solution (mol/L), and 35 is the equivalent weight of B_2O_3.

The dissolution fractions obtained in this way were used in modeling using the Statistica 10 package program. The exponential constants a, b, d, g, m in the kinetic model, Arrhenius constant (A), regression coefficient (r^2) value, and the kinetic model were statistically calculated with the help of the Statistica 10 package program, which works on multiple simultaneous regressions.

RESULTS AND DISCUSSION

Reactions

PA in aqueous solutions ionizes as follows and the acid constant is Ka= $1.34x10^{-5}$.

$CH_3CH_2COOH_{(aq)} + H_2O \longrightarrow CH_3CH_2COO^-_{(aq)} + H_3O^+_{(aq)}$ (5)

When PRG containing SO_2 is passed through this solution, the following reactions occur in addition to reaction 4 [11, 23].

$SO_{2(g)} \leftrightharpoons SO_{2(aq)}$ (6)

$SO_{2(aq)} + 2H_2O \leftrightharpoons H_3O_{(aq)}^+ + HSO_{3(aq)}^-$ (7)

$HSO_{3(aq)}^- + H_2O \leftrightharpoons H_3O_{(aq)}^+ + SO_{3(aq)}^{2-}$ (8)

Under standard conditions, for reaction 6, K_{a1}=1.72 $x10^{-2}$, and for reaction 8, K_{a2}=$6.43x10^{-8}$. When colemanite ore is added to this solution, the $H_3O_{(aq)}^+$ ions forming based on reactions 7 and 8 generate $Ca_{(aq)}^{2+}$ and $H_2B_6O_{11}^{2-}$ ions in reaction 9 below and form H_3BO_3 in solid and solution form through reaction 9.

$Ca_2B_6O_{16}H_{10(s)} + 2H_3O^+_{(aq)} \longrightarrow 2Ca^{2+}_{(aq)} + H_2B_6O_{11}^{2-}{}_{(aq)} + 7H_2O$ (9)

$H_2B_6O_{11(aq)}^{2-} + 2H_3O_{(aq)}^+ + 5H_2O \longrightarrow 6H_3BO_{3\ (aq,s)}$ (10)

Due to reactions 9 and 10, the H_3O^+ ions surrounding the particles reacting reduce and the pH of the medium increases. This results in a slide to the right for the equilibrium in reaction 8 and SO_3^{2-} ion concentrations will increase. In this situation, for the formation of $CaSO_3.{}^1/_2H_2O_{(s)}$, known as hannebachite, the following condition occurs $[Ca_{(aq)}^{2+}][SO_{3(aq)}^{2-}][H_2O]^{0.5}>K_{sp}$ and the following reaction occurs between Ca^{2+} and SO_3^{2-} ions in the medium.

$$Ca_{(aq)}^{2+} + SO_{3(aq)}^{2-} + {}^1/_2H_2O \longrightarrow CaSO_3.{}^1/_2H_2O_{(s)} \quad (11)$$

The total reaction is given below:

$$Ca_2B_6O_{16}H_{10(s)} + 2SO_{2(g)} + 5H_2O \longrightarrow 2(CaSO_3.{}^1/_2H_2O_{(s)}) + 6H_3BO_{3(aq,s)} \quad (12)$$

Thus, a layer consisting of solid boric acid formed according to reaction 10 and calcium sulfite ($CaSO_3.0.5H_2O$) formed according to reaction 11 will form around the unreacted core. $CaSO_3.{}^1/_2H_2O$ is solid and insoluble in water, but solid boric acid is soluble in it. For this reason, at any moment, a tight solid boric acid + $CaSO_3.{}^1/_2H_2O$ layer controlling the reaction rate will form around the unreacted core, and this layer, there will be a porous layer of $CaSO_3.{}^1/_2H_2O$ layer including does not affect on the reaction rate. Both layers contain clay minerals. The dissolution process is given schematically in Figure 4. The X-ray diffraction and SEM image results of the solid residue occurring during experimental studies, seen in Figures 5 (a) and (b) confirm this. The $CaSO_3.{}^1/_2H_2O$ is a valuable by-product. On SEM images, the specific crystal structure for $CaSO_3.{}^1/_2H_2O$ is observed.

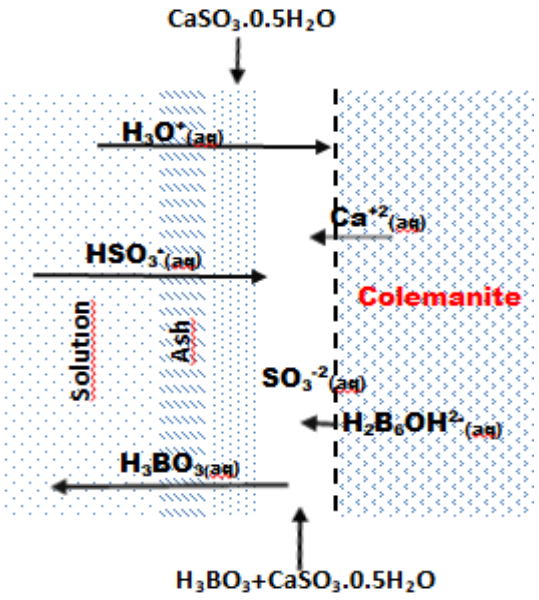

Fig. 4: Schematic view of the dissolution process

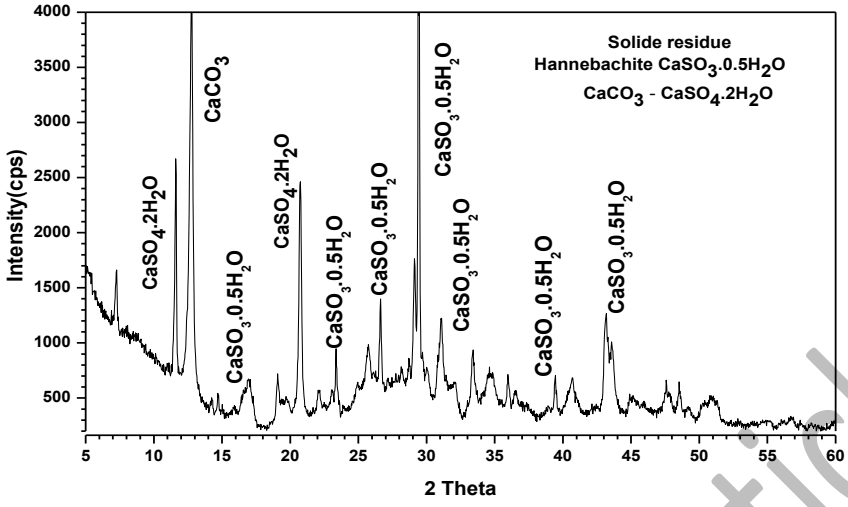

(a)

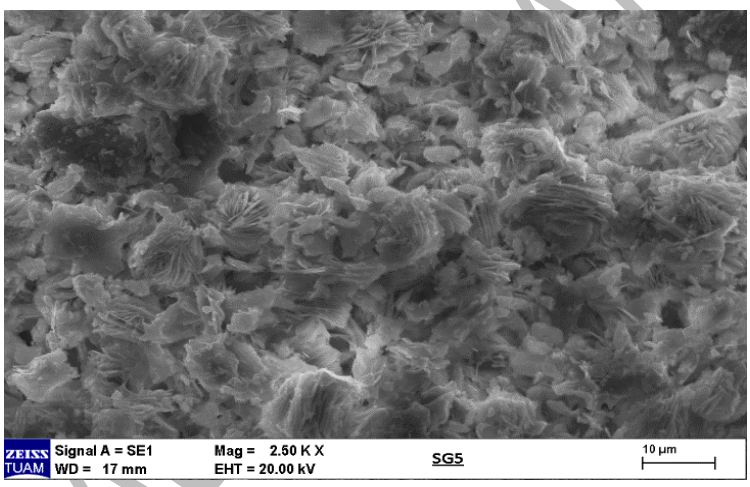

(b)

Fig. 5: X-ray diffractogram (a) and SEM image (b) of the solid residue obtained in experiments

Effect of parameters

To determine the dissolution kinetics for colemanite; the temperature, particle size, solid/liquid ratio, propionic acid concentration, PRG flow rate, and stirring speed were selected as parameters. The levels for each parameter can be seen in Table 2. The values marked with asterisks in Table 3 were used for the fixed-parameter levels during investigating the dissolution kinetics. These Fixed parameter values allowed the ability to observe the effect of the investigated parameter. For kinetic assessments, dissolution fractions calculated according to equation 4 were graphed against time.

Effect of reaction temperature

The dissolution fraction against time is shown as a graph in Figure 6. The effect of reaction temperature on dissolution rate was analyzed. Since the kinetic energy increases exponentially with increasing temperature,

the number of molecular collisions per unit of time will also increase [1, 19]. For this reason, the reaction rate increased with temperature, and hence the amount of B_2O_3 passing into the solution appeared to increase. The fact that the temperature is very sensitive to the dissolution rate is thought to fit the chemical reaction-controlled model of the process [33]. Otherwise, it is concluded that it fits the diffusion-controlled model. Its measure is the value of the activation energy. Activation energies above 40 kJ/mol indicate that the process is chemically controlled, and lower values indicate that it is diffusion-controlled.

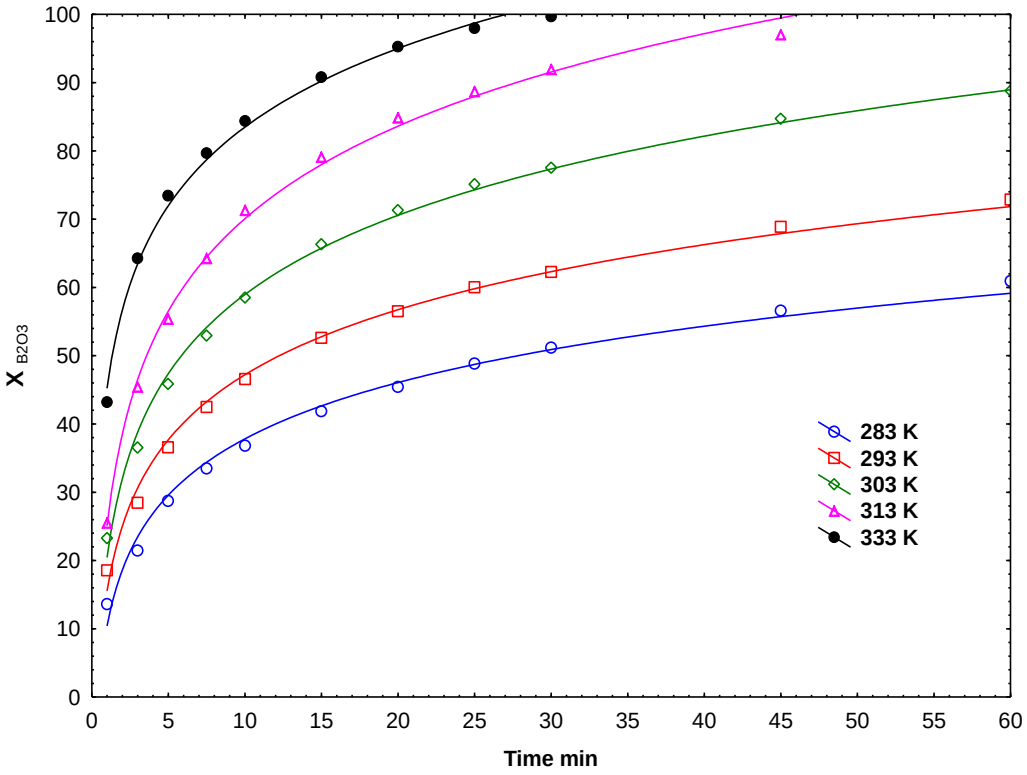

Fig. 6: Effect of temperature on the dissolution rate of colemanite in PA solution saturated with PRG

Effect of particle size

The effect of particle size on the colemanite dissolution rate was investigated with 100-150, 150-250, 250-400, and 400-600 µm fractions. The dissolution fraction against time is given graphically in Figure 7. Decreasing the particle size increases the total surface area in the solution environment. As the surface area increases, the dissolution surface per unit amount of solvent acid and gas naturally increases. Therefore, it is an expected result that the decrease in particle size will increase the dissolution rate.

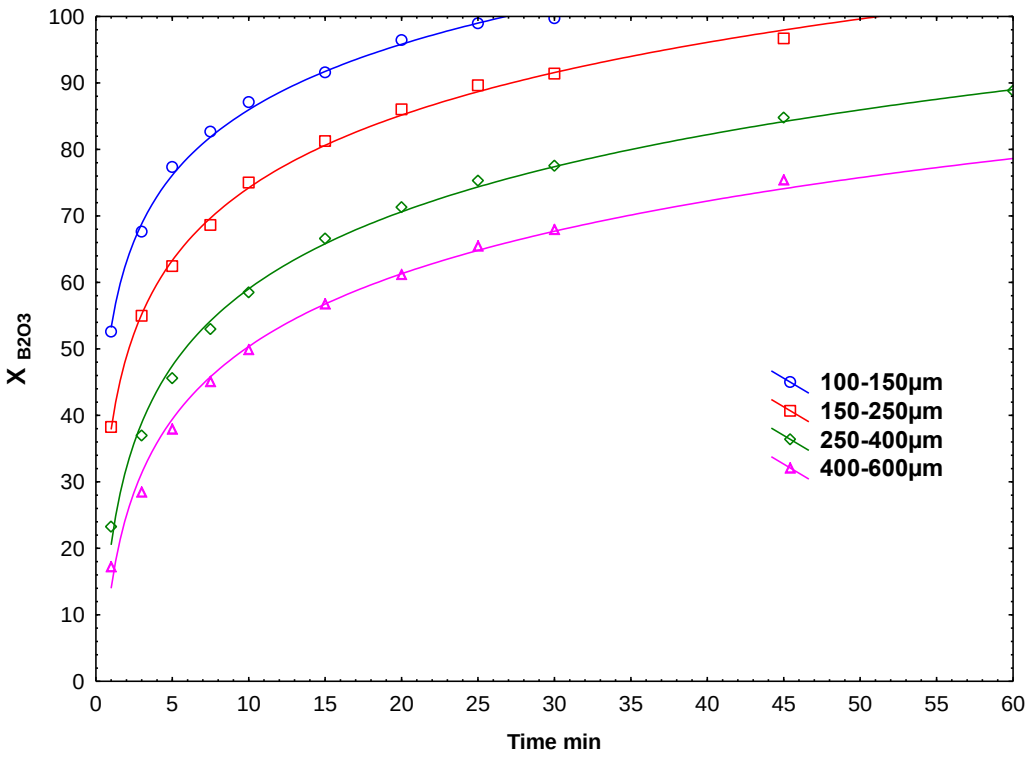

Fig. 7: Effect of particle size on the dissolution of colemanite in PA solution saturated with PRG

Effect of solid-liquid ratio

The effect of the solid-liquid ratio on the dissolution rate of colemanite is investigated using 20, 40, 60 and, 80 g/L values. The dissolution fraction against time is shown graphically in Figure 8. As seen in Figure 8, with the increase in solid/liquid ratio, the dissolution rate appears to reduce due to the increase in solid amount per unit solvent. Approximately 58% of the B_2O_3 in colemanite in 80 g/L solid/liquid ratio in 30 minutes, 68% in 60 g/L and the same time, 78% in 40 g/L and 90% in 20 g/L It is seen that it has passed into a solution. On the other hand, there is an increase in the amount of dissolved solids per unit amount of the solution (Figure 9). Again, when the results obtained in 30 minutes are compared, 15.87 g in 80 g/L solid/liquid ratio, 13.96 g in 60 g/L, 10.4 g in 40 g/L and 20 g/L It is seen that 6.71 g of B_2O_3 has passed into the solution.

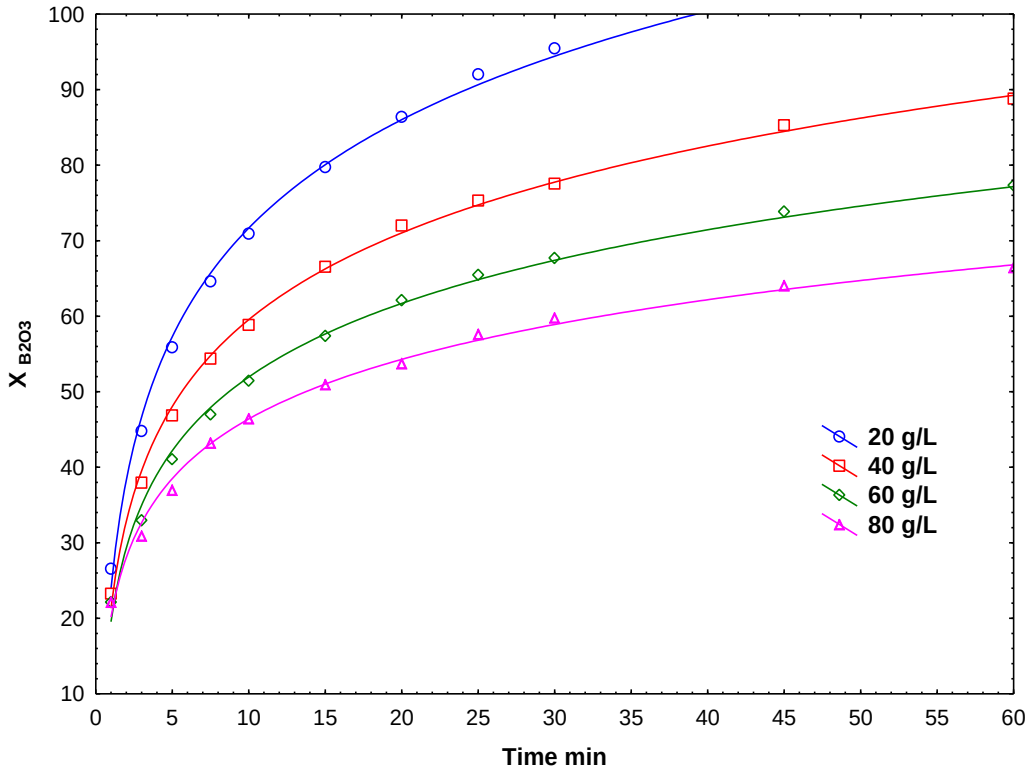

Fig. 8: Effect of solid/liquid ratio on the dissolution of colemanite in PA solution saturated with PRG (as a percent of B_2O_3 passing to the solution)

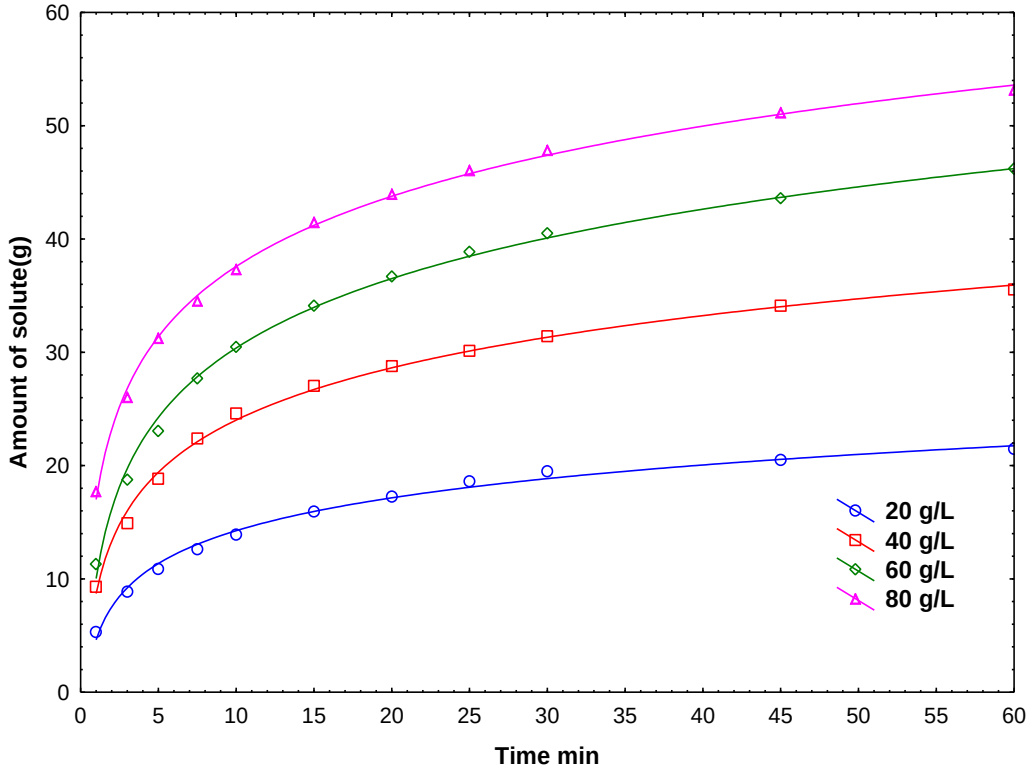

Fig. 9: Effect of solid/liquid ratio on the dissolution of colemanite in PA solution saturated with PRG (as B_2O_3 amount(g) passing to the solution)

Effect of acid concentration

The effect of propionic acid concentration on the dissolution rate of colemanite was examined at different concentrations such that 0%, 2.5%, 5%, and 10% of the total solution amount was acid. The dissolution fraction values against time are given graphically in Figure 10. As seen in Figure 10, the dissolution rate increases with the increase in acid concentration. As the PA concentration increases, the active H_3O^+ ion concentration, which enters the solution environment and is effective in the dissolution process, increases continuously according to equation 5. Therefore, the concentration of H_3O^+ ions that encounter colemanite in unit volume and unit time increases, and the effective penetration of these increasing ions into the colemanite ore causes more ore to dissolve and the dissolution rate to increase. A striking point here is the absence of PA in the environment. In this case, the dissolution behavior is quite different from the others and the dissolution rate is quite low compared to other states. In this case, the only source of H_3O^+ ions is sulfurous acid according to equations 7 and 8, and Ca^{2+} formed according to equation 9 and SO_3^{2-} formed according to equation 8 form solid $CaSO_3.{}^1/_2H_2O$ (hannabachite) according to equation 11.

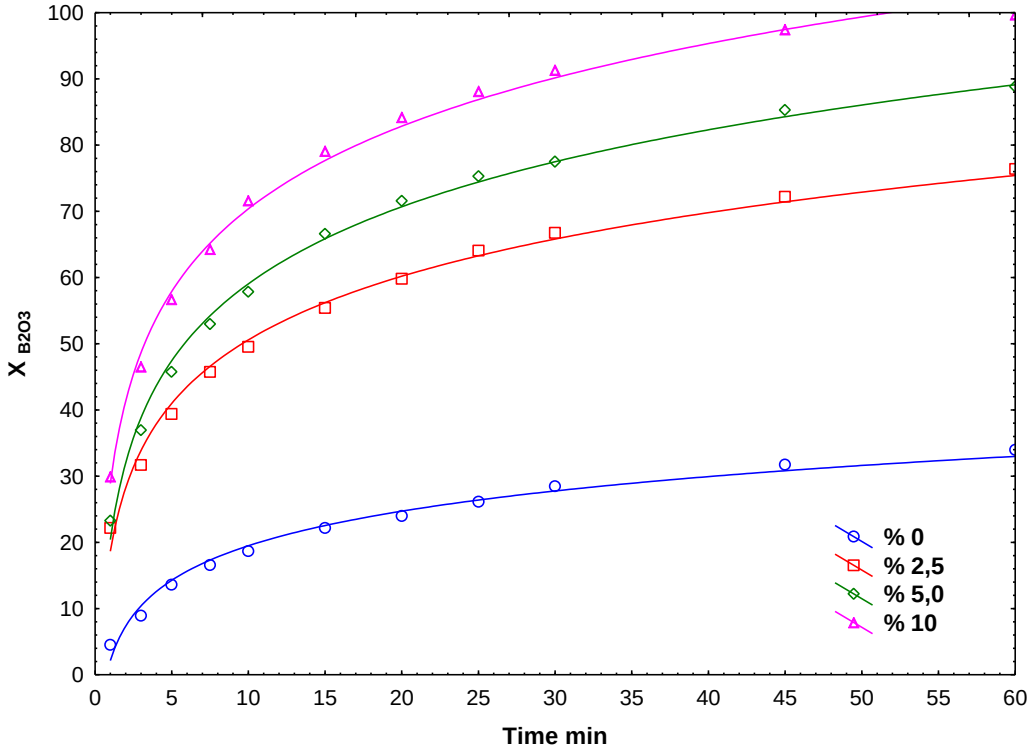

Fig. 10: Effect of PA concentration on dissolution of colemanite in PA solution saturated with PRG

This solid formation adheres to the unreacted particle and reduces the reaction rate. In cases where PA is used, in addition to equations 7 and 8, according to reaction 5, the H_3O^+ and $CH_3CH_2COO^-$ are formed, however, $CH_3CH_2COO^-$ ion passes into the main solution, while H_3O^+ ion reacts with colemanite according to equation 9 and Ca^{2+} ion is formed. In addition, equation 8 shifts to the left due to the excess H_3O^+ formed according to equation 5, SO_3^{2-} concentration decreases, and HSO_3^- concentration increases. As a result, the solid $CaSO_3.{}^1/_2H_2O$ formed around the unreacted core according to equation 11 has a more porous structure than the case without PA. Therefore, the dissolution reaction takes place faster.

Effect of gas flow rate

The effect of PRG flow rate on colemanite dissolution rate was examined at flow rates of 50, 100, and 150 mL/min. The graph of dissolution fraction values against time is shown in Figure 11. As seen in Figure 11, as the gas flow rate increased, the dissolution rate increased. Here, the increase in PRG flow rate increased the H_3O^+ ion concentration in the solute according to reactions 5 and 6; this caused an increase in the dissolution rate of colemanite.

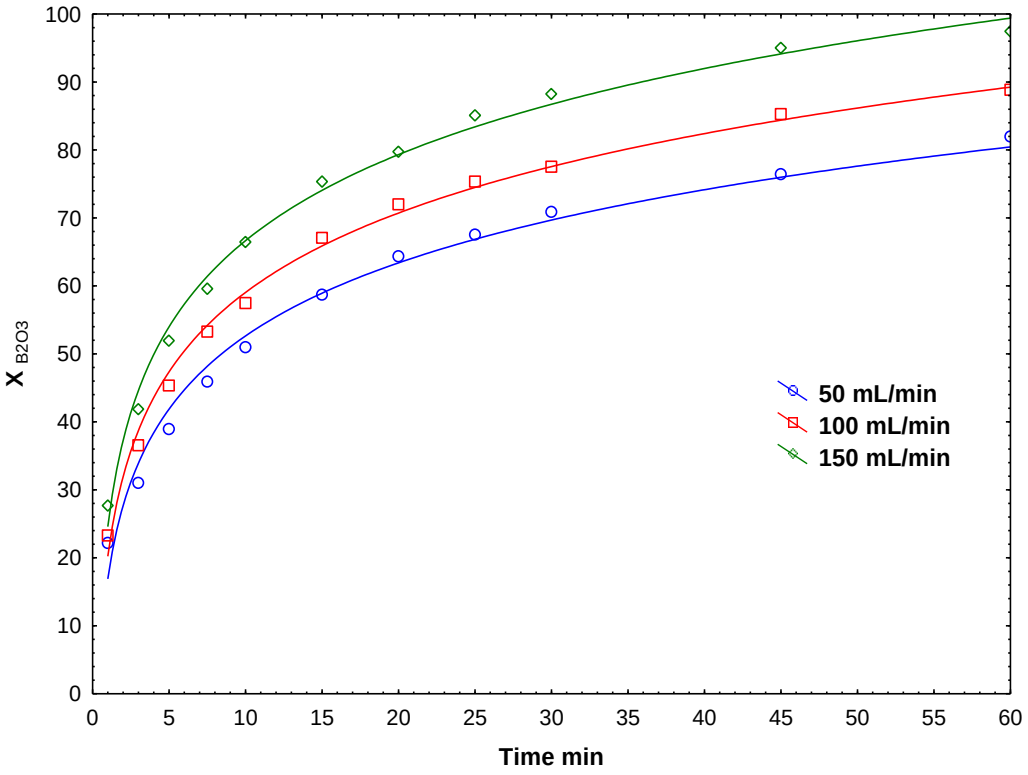

Fig. 11: Effect of PRG flow rate on the dissolution of colemanite in PA solution saturated with PRG

Effect of stirring speed

The effect of the stirring speed was investigated at 300, 400, and 500 rpm. The results are given in Figure 12 as dissolution fractions against time. The lowest stirring speed of 300 rpm was the lowest rate ensuring full mixing and was identified in preliminary experiments. Figure 12 shows that increasing the stirring speed from 300 rpm to 400 rpm does not have much effect on the dissolution rate. At the end of the 60th minute, it is seen that the dissolution rate is 90.8% at 400 rpm stirring speed, while it is 96.52% at 500 rpm stirring speed. An increase of approximately 6.1% in the dissolution rate was observed when increasing from 400 to 500 rpm. This was due to the effectiveness of fluid-solid contact by thinning the fluid film layer. Compared to other parameters, the effect of stirring speed on the dissolution rate is much lower.

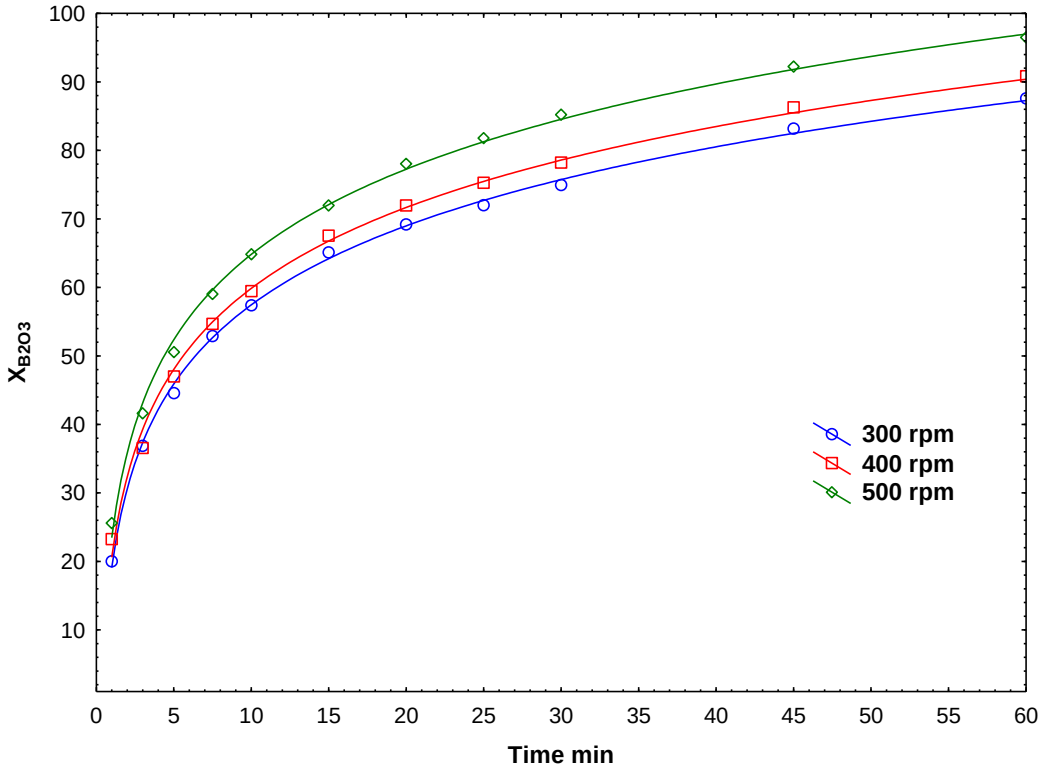

Fig. 12: Effect of stirring speed on the dissolution of colemanite in PA solution saturated with PRG

Kinetic analysis

Kinetics studies the effects of various parameters on reaction rates. Such information can be used for equipment in plant design. In this respect, it is important to conduct kinetic studies of a reaction [32]. Fluid-solid non-catalytic reaction kinetics can be explained according to heterogeneous and homogeneous reaction models [18]. In the homogeneous reaction model, it is assumed that a liquid containing the reactant permeates every point of the solid, and reacts with it. In the heterogeneous model, fluid reactant reaches the unreacted core surface in three stages. First, the reactant passes through a fluid film and then an ash or product film, and when the external surface of the unreacted core reaches, the reaction occurs with the solid. In this process, the stage with the highest resistance is assumed to control the reaction rate [25].

Determination of the kinetic model

In previous studies, the dissolution of pure colemanite mineral and ore in aqueous environment with pure SO_2 gas was investigated. When pure colemanite ore was used, the reaction activation energy was determined as 53.97 kJ/mol, and the reaction was determined to comply with the chemical reaction-controlled model [34]. It was found that 39.53 kJ/mol activation energy and chemical reaction control [26].

Attempts were made to explain the dissolution kinetics and rate control step for the dissolution of colemanite ore in PA solutions saturated with PRG using the homogeneous and heterogeneous reaction models. Analysis of experimental results was performed graphically and statistically. To determine which model controlled the process rate, the dissolution fraction values for all parameters, apart from stirring speed which did not affect dissolution fraction, and 0% of PA concentration which behaves differently from other PA concentrations, were used in the reaction rate equations. The r^2 (regression) values were found and given in Table 3.

Table 3: r^2 values for rate equations in trialed models

Equations	Type of rate control	r^2
$kt = 1 - 3(1-X)^{2/3} + 2(1-X)$	Ash film diffusion control for fixed-size spheres	0.939
$kt = 1 - (1-X)^{1/3}$	Chemical reaction control for fixed-size spheres	0.811
$kt = 1 - (1-X)^{1/2}$	Fluid film diffusion control for shrinking spheres (large grain)	0.612
$kt = 1 - (1-X)^{2/3}$	Fluid film diffusion control shrinking spheres (small grain)	0.37
$kt = -\ln(1-X)$	First-order pseudo homogenous reaction model	0.948
$kt = X/(1-X)$	Second-order pseudo homogenous reaction model	0.729
$kt^m = -\ln(1-X)$	Avrami model	0.979
$kt = X^2$	Ash film diffusion control for fixed-size flat plate	0.819
$kt = X + (1-X)\ln(1-X)$	Ash film diffusion control for fixed-size cylinder	0.912
$kt^m = 1 - 3(1-X)^{2/3} + 2(1-X)$	**Modified Avrami model**	**0.986**

When the highest r^2 values in Table 3 are investigated, the rate expression for the process appears to abide by the modified Avrami model. To confirm the results related to this model with statistical analyses, the effects of each parameter on the model equation were investigated. The reaction rate expression for the modified Avrami model is given in Equation 12.

$$kt^m = 1 - 3(1-X)^{2/3} + 2(1-X) \quad (12)$$

As seen in Equation 12, considering the reality that the graph of $\ln[1 - 3(1-X)^{2/3} + 2(1-X)]$ against lnt must be linear and parallel for every parameter. Figures 13-17 show the $\ln[1 - 3(1-X)^{2/3} + 2(1-X)]$ against lnt graphs for reaction temperature, particle size, solid/liquid ratio, propionic acid concentration, and PRG flow rate, respectively. The linear and parallel lines obtained from these graphs show the process is controlled by the modified Avrami model.

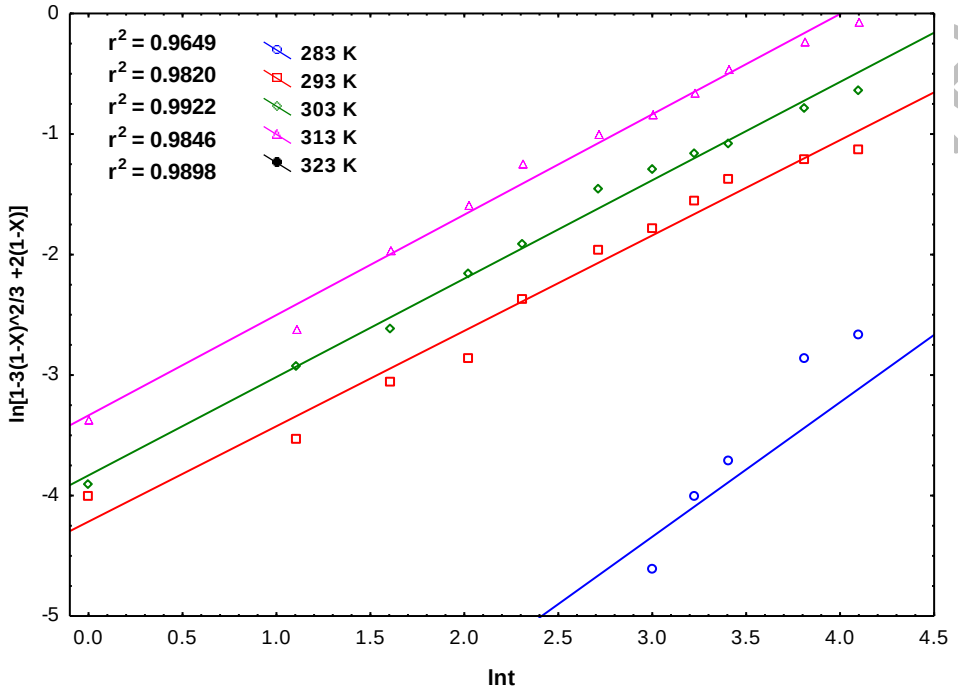

Fig. 13: Variation of $\ln[1 - 3(1-X)^{2/3} + 2(1-X)]$ against lnt for different reaction temperatures

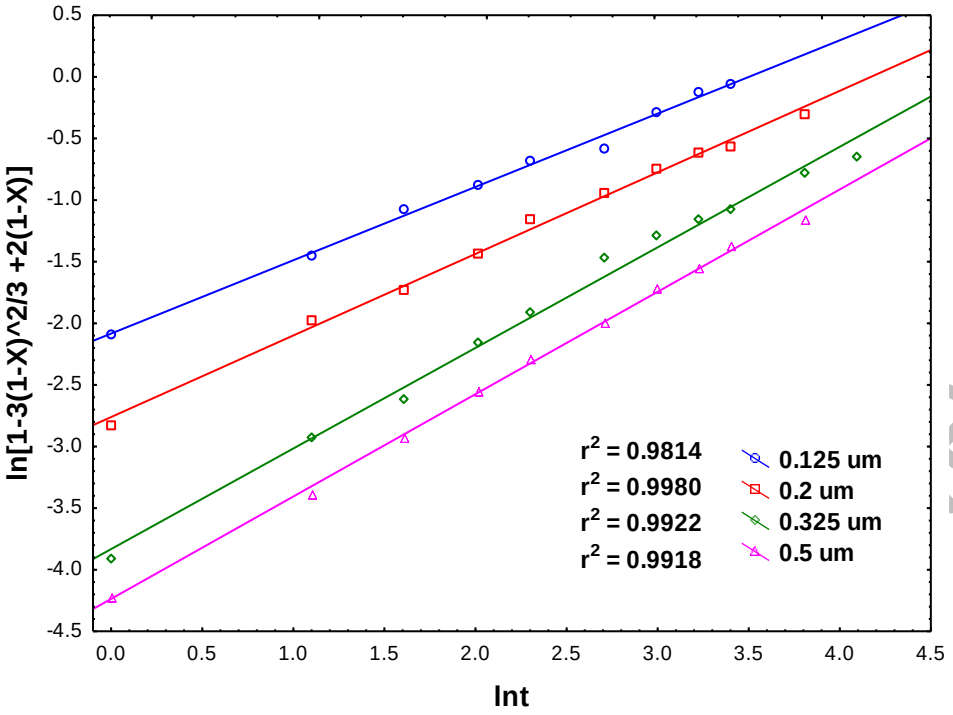

Fig. 14: Variation of ln[1 - 3(1-X)$^{2/3}$ + 2(1-X)] against lnt for different particle sizes

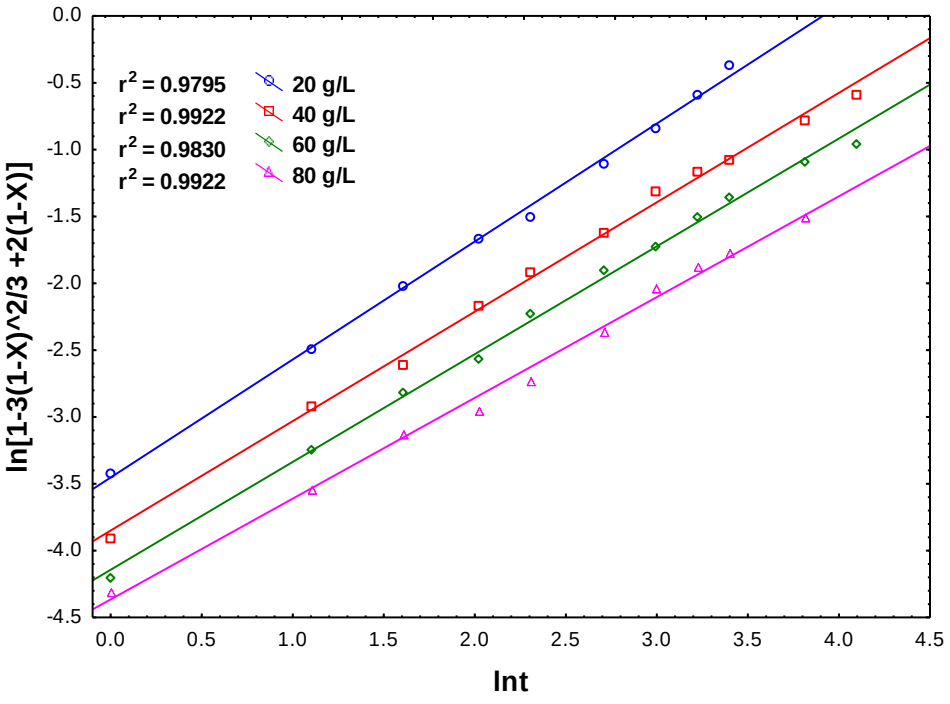

Fig. 15: Variation of ln[1 - 3(1-X)$^{2/3}$ + 2(1-X)] against lnt for different solid-liquid ratios

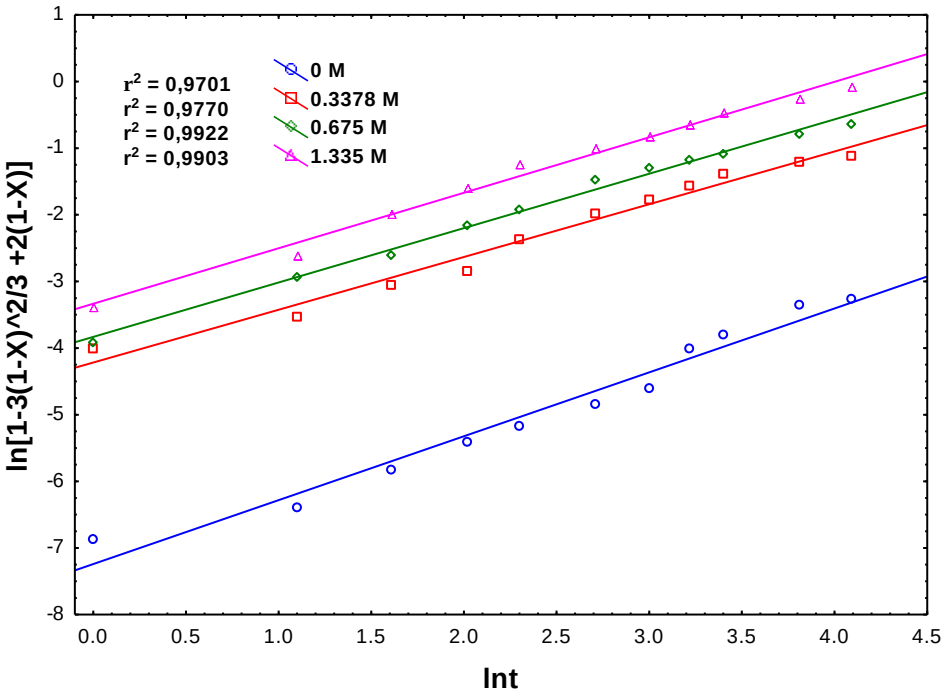

Fig. 16: Variation of ln[1 - 3(1-X)$^{2/3}$ + 2(1-X)] against lnt for different propionic acid concentrations

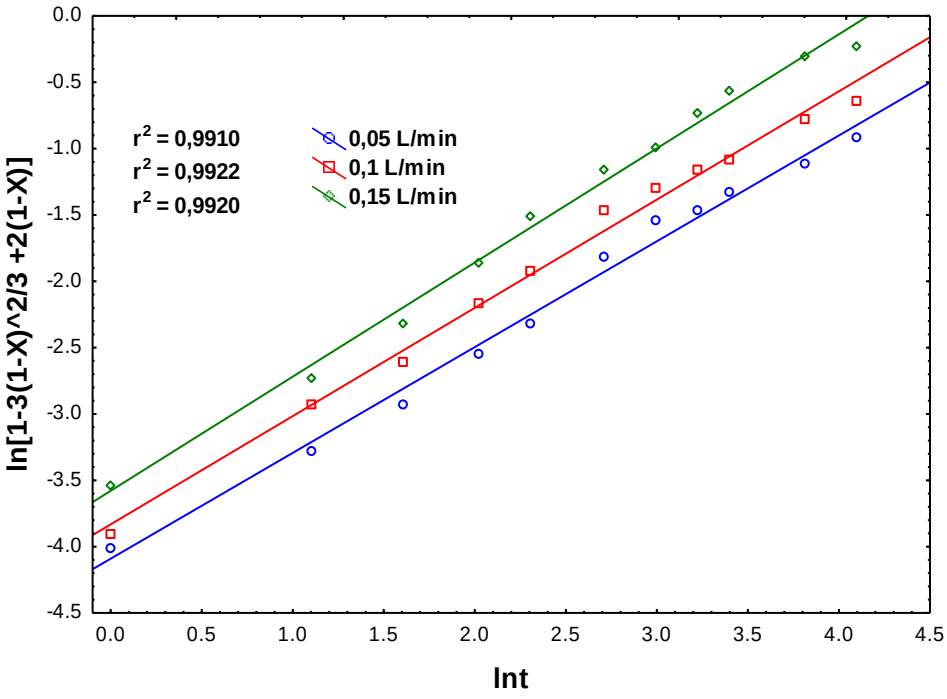

Fig. 17: Variation of ln[1 - 3(1-X)$^{2/3}$ + 2(1-X)] against lnt for different PRG flow rates

Determination of activation energy and Arrhenius constant

The reaction rate constant, k, in equation 13 is determined by the point where the line obtained for each temperature line in Figure 13 intersects the ordinate (ln k). The reaction rate constant is linked to temperature and the Arrhenius equation can be used to determine the correlation between k and T [35, 36]:

$k=Ae^{-E/RT}$ (14)

By taking the natural logarithm of both sides in Equation 14, Equation 15 is obtained.

$$\ln k = \ln A - \frac{E}{RT} \quad (15)$$

The reaction activation energy is determined by the slope of the graph of lnk against 1/T(K) [37]. The Arrhenius graph is shown in Figure 18.

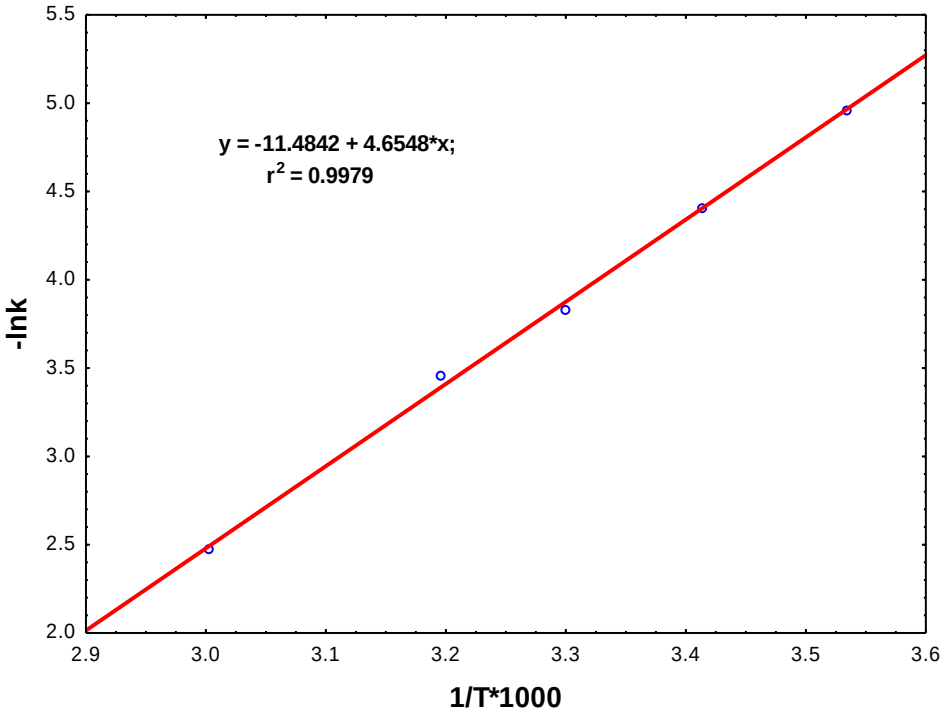

Fig. 18: lnk against 1/T(K)*1000 (Arrhenius graph)

The slope of the straight line in the Arrhenius graph indicates the activation energy (E) is 38.66 kJ/mol and the Arrhenius constant (A) is $9.6*10^4$. The determination of the activation energy of the process as 38.66 kJ/mol, that is, not above 40 kJ/mol, confirms that the dissolution rate of the process is controlled by diffusion from the modified Avrami model.

The dependence of the rate constant (k) in the modified through Avrami model flow model in Equation 13 on the parameters, solid/liquid ratio, particle size, propionic acid concentration, and PRG flow rate, is given by Equation 15.

$k = A.\ (KS)^a\ .(D)^b\ .(C)^d\ .(GD)^g.\ e^{-E/RT}$ (16)

When Equation 13 and Equation 16 for the modified Avrami model are combined, Equation 17 is obtained.

$1 - 3(1-X_{B_2O_3})^{2/3} + 2(1-X_{B_2O_3}) = A.\ (KS)^a.\ (D)^b.\ (C)^d.\ (GD)^g.\ e^{-E/RT}\ .t^m$ (17)

Here, a, b, d, g, and m were exponential constants determined by statistical calculations with multiple simultaneous regression using the Statistica 10 program. Constants a, b, d, g, and m in equation (17) were

determined to be -0.94, -1.06, 0.73, 0.77 and 0.7, respectively. When these results are inserted into Equation 16, the modified Avrami model equation given in Equation 18 is obtained.

$$1 - 3(1-X_{B_2O_3})^{2/3} + 2(1-X_{B_2O_3}) = 9.6*10^4\,(KS)^{-0.94}.\,(D)^{-1.06}.\,(C)^{0.73}.(GD)^{0.77}.e^{-38.66/RT}t^{0.7} \quad (18)$$

Validation of the kinetic model

According to the reaction rate model, the $X_{experimental}$ results versus $X_{theoretical}$ results obtained from the Statistica 10 program were graphed in Figure 19 and the fit of the model was investigated. The theoretical dissolution values versus experimental dissolution values lining up along the same diagonal or close to the diagonal indicate that the theoretical results in the model chosen for this process and the experimental results have a good fit with each other.

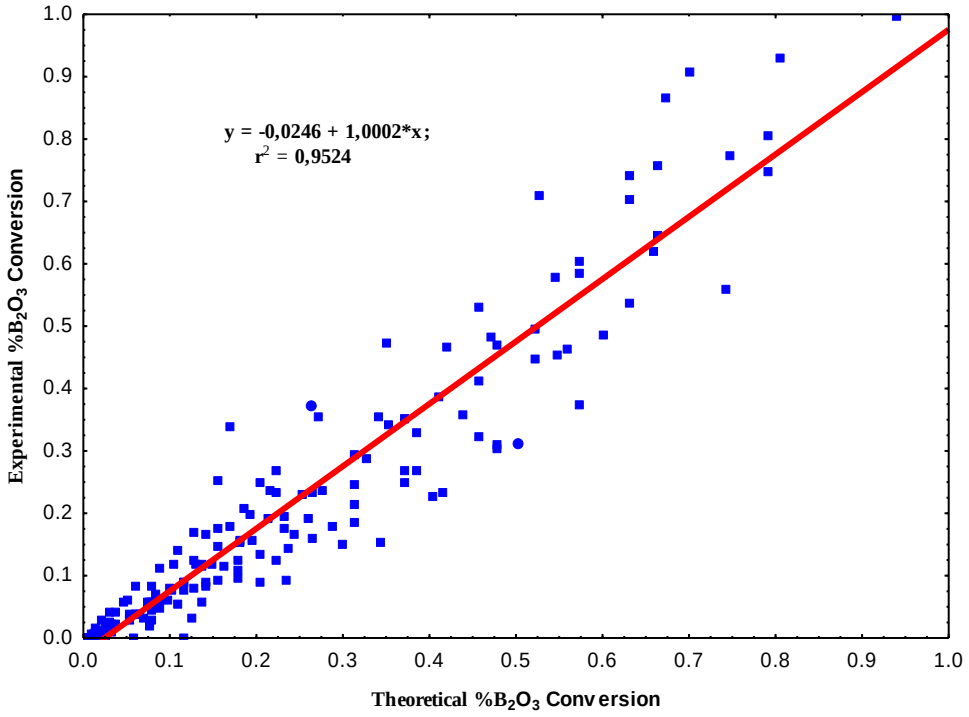

Fig. 19: Comparison of experimental dissolution values with theoretical dissolution values

CONCLUSIONS

This study investigated the dissolution kinetics of colemanite in a propionic acid solution saturated with PRG at atmospheric pressure and attempted to identify an alternative reactant for boric acid production. The effects of the selected parameters on colemanite dissolution rate and related results can be stated as follows:

- ✓ The dissolution rate increases proportionally with the reaction temperature, PRG flow rate, and propionic acid concentration. As the reaction temperature increases, the number of molecule collisions per unit time also increases. Thus, the kinetic energy value increases exponentially. For this reason, the reaction rate increased with temperature, and hence the amount of B_2O_3 passing into the solution appeared to increase. The increase in PRG flow rate increased the H_3O^+ ion concentration in the solute; this caused an increase in the dissolution rate of colemanite. As the concentration of propionic acid in

the solution increases, the active H_3O^+ ion concentration, which passes into the solution medium and is effective in the dissolving process, constantly increases. These increased ions cause more ore to dissolve per unit of time, and thus, the dissolution rate increases.

- ✓ It is observed that the dissolution rate increases as the solid/liquid ratio decreases. Increasing the solid/liquid ratio causes an increase in the amount of solid colemanite particles per non-reactive PRG and propionic acid solvent in the reaction mixture and a decrease in the dissolution rate. Increasing the solid/liquid ratio increases the amount of solid colemanite particles per amount of unreactive PRG and propionic acid solvent in the reaction mixture and decreases the dissolution rate. This reduces the rate of B_2O_3 passing into the solution and increases the rate of staying solid. On the other hand, there is an increase in the amount of dissolved solids per unit amount of the solution. The decrease in particle size of colemanite in solution causes an increase in total surface area in solution. As the surface area increases, the particles per unit amount of the suspension, which naturally consists of PRG and propionic acid solution, form a high contact area. Thus, an increase in the rate of B_2O_3 passing into the solution is observed. It was observed that the increase in stirring speed at a certain rpm did not cause a significant increase in dissolution. In addition, it has been observed that increasing the stirring speed to a certain extent positively increases partial dissolution. However, the effect of stirring speed on dissolution was found to be minimal and negligible compared to other parameters.
- ✓ We determine that propionic acid and PRG, which have a weakly acidic structure, can dissolve colemanite ore for the production of boric acid. Thus, solvent reactants are determined for boric acid with higher purity, no added value byproduct ($CaSO_3.{}^1/_2H_2O$), and no environmentally hazardous waste production.
- ✓ The modified Avrami model $kt^m = - \ln [1 - 3(1-X)^{2/3} + 2(1-X)]$ was the most suitable model and the process was determined to have 38.66 kJ/mol activation energy. This activation energy, the linear portions of the graphs in Figures 13-17, and the fit of experimental values with theoretical values in Figure 19 confirm the suitability of this model. During the process, the ash comprising clay minerals remaining from the dissolved colemanite along with the formation of crystalline boric acid and crystalline hannebachite ($CaSO_3.{}^1/_2H_2O$) support the suitability of the modified Avrami model.
- ✓ The mathematical model linked to the effect of the selected parameters was determined below: and the regression value of the model (r^2) was calculated as 0.986.

$$1 - 3(1-X_{B_2O_3})^{2/3} + 2(1-X_{B_2O_3}) = 9.6*10^4\,(KS)^{-0.94}.\,(D)^{-1.06}.\,(C)^{0.73}.(GD)^{0.77}.\,e^{\frac{-38.66}{R*T}}.t^{0.7}$$

Acknowledgments

This study was supported by Çankırı Karatekin University. The author thanks Prof. Dr. M. Muhtar KOCAKERİM and Assoc. Prof. Dr. Barış ŞİMŞEK for support and helpful discussions.

Nomenclature

K_a Ionization constant

X Conversion fraction

t Reaction time (min)

T Reaction temperature (K)

S Solid amount (g)

L Liquid amount(mL)

D Mean particle size (μm)

R Universal gas constant (8.314 kJ/mol)

r^2 Regression coefficient

k Reaction rate constant

E Activation energy

A Frequency factor

a, b, d, g, m Model constants

C Propionic acid concentration (M)

GD Gas flow rate (mL/min)

PA Propionic acid

PRG Pyrite roasting gas

Indexes

s solid

aq aqueous solution

Appendix

Table A1: Kinetic study experiment plan

Experiment No.	Reaction temperature (K)	Particle size (µm)	Solid/fluid ratio (g/L)	Acid concentration (%)	PRG flow (L/min)	Stirring rate (rpm)
1	**283**	250-400	40	5	100	400
2	**293**	250-400	40	5	100	400
3	**303**	250-400	40	5	100	400
4	**313**	250-400	40	5	100	400
5	**323**	250-400	40	5	100	400
6	303	**100-150**	40	5	100	400
7	303	**150-250**	40	5	100	400
8	303	**400-600**	40	5	100	400
9	303	250-400	**20**	5	100	400
10	303	250-400	**60**	5	100	400
11	303	250-400	**80**	5	100	400
12	303	250-400	40	**0**	100	400
13	303	250-400	40	**2,5**	100	400
14	303	250-400	40	**10**	100	400
15	303	250-400	40	5	**50**	400
16	303	250-400	40	5	**150**	400
17	303	250-400	40	5	100	**300**
18	303	250-400	40	5	100	**500**

REFERENCES

[1] Şimşek H.M., Guliyev R., Beşe A.V., Dissolution Kinetics of Borogypsum in Di-Ammonium Hydrogen Phosphate Solutions, İnternational Journal of Hydrogen Energy, 43(44):20262-20270 (2018).
[2] Kopac T., Kırca Y., Toprak A., Synthesis and Characterization of KOH/Boron Modified Activated Carbons From Coal and Their Hydrogen Sorption Characteristics, International Journal of Hydrogen Energy, 42(37):23606-23616 (2017).
[3] Kucuk V., Kocakerim M.M., Effects of Leaching Parameters on The İmpurity İon Concentrations at Ulexite Ore Leaching: An Experimental Design Approach, Iranian Journal of Chemistry and Chemical Engineering (IJCCE), 38(3):245-255 (2019).
[4] Şimşek H.M., Guliyev R., A Taguchi Optimization Study About The Dissolution of Colemanite in Ammonium Bisulfate (NH_4HSO_4) Solution, Iranian Journal Chemistry and Chemical Engineering (IJCCE), 41(8): 2735-2742 (2022).
[5] Tunç M., Yapıcı S., Kocakerim M.M., Yartasi A., The Dissolution Kinetics of Ulexite in Sulphuric Acid Solutions, **Chemical and Biochemical Engineering Quarterly**, 15(4):175-180 (2001).
[6] Mergen A., Demirhan M., Dissolution Kinetics of Probertite in Boric Acid Solution, International Journal of Mineral Processing, 90(1-4):16-20 (2009).
[7] Tunç M., Dissolution Kinetics of Ulexite in Phosphoric Acid, Asian Journal of Chemistry, 20(4):3161-3170 (2008).
[8] Türkaslan B,E., Dalbeyler A., An Alternative Pre-treatment Sterilization Solution Synthesis Utilizing Boric Acid Doped Graphene Oxide, Iranian Journal of Chemistry and Chemical Engineering (IJCCE), 41(11):3638-3645 (2022).
[9] Fu Q., Rahaman M.N., Fu H., Liu X., Silicate, Borosilicate, And Borate Bioactive Glass Scaffolds With Controllable Degradation Rate For Bone Tissue Engineering Applications. I. Preparation and in Vitro Degradation. Journal of Biomedical Materials Research Part A, 95(1):164-171 (2010).
[10] Arasu A.V., Sornakumar T., Design, Manufacture and Testing of Fiberglass Reinforced Parabola Trough For Parabolic Trough Solar Collectors, Solar Energy, 81(10):1273-1279 (2007).
[11] Tunç M., Kocakerim M.M., Küçük Ö., Aluz M., Dissolution of Colemanite in $(NH_4)_2SO_4$ Solutions, Korean Journal of Chemical Engineering, 24(1):55-59 (2007).
[12] Kizilca M., Copur M., Kinetic İnvestigation of Reaction Between Colemanite Ore and Methanol, Chemical Engineering Communications, 202(11):1528-1534 (2015).
[13] Küçük N., Küçük Ö., Solak A.O., Optimization by Using the Taguchi Method of Boric Acid Production by Dissolving Flash Calcined Colemanite in Water Saturated with SO_2, Iranian Journal of Chemistry and Chemical Engineering (IJCCE), 42(127):1597-1611 (2023).
[14] Guliyev R., Kuşlu S., Çalban T., Çolak S., Leaching Kinetics of Colemanite in Ammonium Hydrogen Sulphate Solutions, Journal of Industrial and Engineering Chemistry, 18(4):1202-1207 (2012).
[15] Tunc M., Irem H., Kocakerim M.M., Copur M., Küçük Ö., The Conversion Kinetics of Tincal to Boric Acid in Nitric Acid Solutions, Iranian Journal of Chemistry and Chemical Engineering (IJCCE), 39(2):83-90 (2020).
[16] Davies T., Colak S., Hooper R., Boric Acid Production By The Calcination and Leaching of Powdered Colemanite, Powder Technology, 65(1-3):433-440 (1991).
[17] Go□nen M., Nyankson E., Gupta R.B., Boric Acid Production From Colemanite Together With Ex Situ CO_2 Sequestration, Industrial & Engineering Chemistry Research, 55(17):5116-5124 (2016).
[18] Karagöz Ö., Kuşlu S., Dissolution Kinetics of Colemanite in Potassium Dihydrogen Phosphate Solution (KH_2PO_4), International Journal of Hydrogen Energy, 42(36):23250-23259 (2017).
[19] Bayca S.U., Kocan F., Abali Y., Dissolution of Colemanite Process Waste İn Oxalic Acid Solutions, Environmental Progress & Sustainable Energy, 33(4):1111-1116 (2014).
[20] Ku□nku□l A., Aslan N.E., Ekmekyapar A., Demirkıran N., Boric Acid Extraction from Calcined Colemanite With Ammonium Carbonate Solutions, Industrial & engineering Chemistry Research, 51(9):3612-3618 (2012).
[21] Gür A., Alkan M.E., Leaching Kinetics of Colemanite in Perchloric Acid Solutions, Journal of Chemical Engineering of Japan, 41(5):354-360 (2008).
[22] Gür A., Dissolution Mechanism of Colemanite in Sulphuric Acid Solutions, Korean Journal of Chemical Engineering, 24(4):588-591 (2007).
[23] Kurtbaş A., Kocakerim M.M., Küçük Ö., Yartaşı A., Dissolution of Colemanite in Aqueous Solutions Saturated With Both Sulfur Dioxide (SO_2) Gas and Boric Acid, Industrial & Engineering Chemistry Research, 45(6):1857-1862 (2006).
[24] Çavuş F., Kuşlu S., Dissolution Kinetics of Colemanite in Citric Acid Solutions Assisted By Mechanical Agitation and Microwaves, Industrial & Engineering Chemistry Research, 44(22):8164-8170 (2005).
[25] Alkan M., Doğan M., Dissolution Kinetics of Colemanite in Oxalic Acid Solutions, Chemical Engineering and Processing: Process Intensification, 43(7):867-872 (2004).

[26] Küçük Ö., Kocakerim M.M., Yartaşı A., Çopur M., Dissolution of Kestelek's Colemanite Containing Clay Minerals in Water Saturated With Sulfur Dioxide, Industrial & Engineering Chemistry Research, 41(12):2853-2857 (2002).
[27] Temur H., Yartaşı A., Çopur M., Kocakerim M.M., The Kinetics of Dissolution of Colemanite in H_3PO_4 Solutions, Industrial & Engineering Chemistry Research, 39(11):4114-4119 (2000).
[28] Ceyhun I., Kocakerim M.M., Saraç H., Çolak S., Dissolution Kinetics of Colemanite in Chlorine Saturated Water. Theoretical Foundations of Chemical Engineering, 33(3):253-257 (1999).
[29] Özmetin C., Kocakerim M.M., Yapıcı S., Yartaşı A., A Semiempirical Kinetic Model For Dissolution of Colemanite in Aqueous CH_3COOH Solutions. Industrial & Engineering Chemistry Research, 35(7):2355-2359 (1996).
[30] Kum C., Alkan M., Kocakerim M.M., Dissolution Kinetics of Calcined Colemanite in Ammonium Chloride Solution, Hydrometallurgy, 36(2):259-568 (1994).
[31] Bulutcu A., Ertekin C., Celikoyan M.K., Impurity Control in The Production of Boric Acid From Colemanite in The Presence of Propionic Acid, Chemical Engineering and Processing: Process Intensification, 47(12):2270-2274 (2008).
[32] Austin G.T., "Shreve's chemical process industries", McGraw-Hill Companies, Singapore (1984).
[33] Doğan H.T., Yartaşı A., Kinetic İnvestigation of Reaction Between Ulexite Ore and Phosphoric Acid, Hydrometallurgy, 96(4):294-299 (2009).
[34] Kocakerim M.M., Alkan M., Dissolution Kinetics of Colemanite in SO_2 Saturated Water, Hydrometallurgy, 19(3):385-392 (1988).
[35] Abanades S., Kimura H., Otsuka H., Kinetic İnvestigation of Carbon-Catalyzed Methane Decomposition in A Thermogravimetric Solar Reactor, International Journal of Hydrogen Energy, 40(34):10744-10755 (2015).
[36] Naktiyok J., Bayrakçeken H., Özer A.K., Gülaboğlu M.Ş., Kinetics of Thermal Decomposition of Phospholipids Obtained From Phosphate Rock, Fuel Processing Technology, 116:158-164 (2013).
[37] Kuşlu S., Dişli F.Ç., Çolak S., Leaching Kinetics of Ulexite in Borax Pentahydrate Solutions Saturated With Carbon Dioxide, Journal of Industrial and Engineering Chemistry, 16(5):673-678 (2010).